

Eco-WakeLoc: An Energy-Neutral and Cooperative UWB Real-Time Locating System

Silvano Cortesi[✉], Graduate Student Member, IEEE, Lukas Schulthess[✉], Graduate Student Member, IEEE, Davide Plozza[✉], Graduate Student Member, IEEE, Christian Vogt[✉], Member, IEEE, and Michele Magno[✉], Senior Member, IEEE

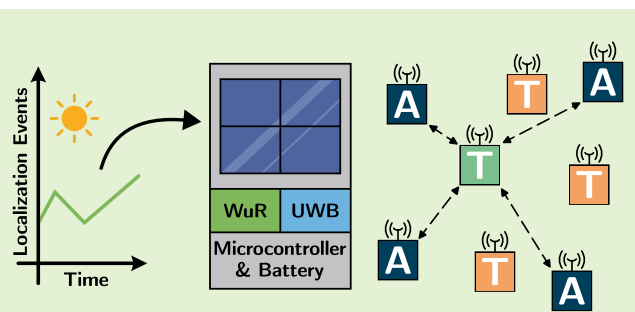
Abstract— Indoor localization systems face a fundamental trade-off between energy efficiency and responsiveness, which is especially important for emerging use cases such as mobile robots operating in GPS-denied environments. Traditional real-time locating system (RTLS) either require continuously powered infrastructure, limiting their scalability, or are limited by their responsiveness. This work presents Eco-WakeLoc, designed to achieve centimeter-level ultra-wideband (UWB) localization while remaining energy-neutral by combining ultra-low power wake-up radios (WuRs) with solar energy harvesting. By activating anchor nodes only on demand, the proposed system eliminates constant energy consumption while achieving centimeter-level positioning accuracy.

To reduce coordination overhead and improve scalability, Eco-WakeLoc employs cooperative localization where *active* tags initiate ranging exchanges, while *passive* tags opportunistically reuse these messages for time difference of arrival (TDOA) positioning. An additive-increase/multiplicative-decrease (AIMD)-based energy-aware scheduler adapts localization rates according to the harvested energy, thereby maximizing the overall performance of the sensor network while ensuring long-term energy neutrality.

A comprehensive evaluation demonstrates centimeter-level accuracy with average errors in 3D space of 21.89 cm for *active* tags using Levenberg-Marquardt trilateration, and 25.70 cm for *passive* tags through cooperative TDOA. The measured energy consumption is only 3.22 mJ per localization for *active* tags, 951 μ J for *passive* tags, and 353 μ J for anchors. Real-world deployment on a quadruped robot with nine anchors confirms the practical feasibility, achieving an average accuracy of 43 cm in dynamic indoor environments. Year-long simulations starting from an empty battery, and using solar harvesting from a 10 cm^2 cell under typical indoor lighting conditions, show that tags achieve an average of 2031 localizations per day, while retaining over 7 % battery capacity after one year – demonstrating that the RTLS achieves sustained energy-neutral operation.

Eco-WakeLoc demonstrates that high-accuracy indoor localization can be achieved at scale without continuous infrastructure operation, combining energy neutrality, cooperative positioning, and adaptive scheduling to enable maintenance-free deployments suitable for large-scale Internet of Things applications.

Index Terms— asynchronous, energy-efficient, energy harvesting, event-driven, indoor localization, Internet of Things (IoT), on-demand, real-time locating system (RTLS), self-sustainable, ultra-wideband (UWB), wake-up radio (WuR).



I. INTRODUCTION

Indoor localization is becoming a cornerstone for a wide range of applications, from smart buildings [1] and asset tracking [2] to robotics [3] and pervasive Internet of Things (IoT) service [4]. Overall, these applications require precise, on-demand, and scalable position tracking, while allowing for extended or even self-sustainable operation of the object localizing itself (the tag), as well as the infrastructure (the anchors) [4], [5]. To achieve these goals, advances in localization technologies, ultra-low-power hardware, efficient localization

algorithms, and energy-efficient localization scheduling must be combined to create solid sensing systems for real-time locating systems (RTLSs) [2], [6], [7].

Concerning localization technology, out of the numerous wireless technologies for indoor localization, ultra-wideband (UWB) has emerged as a leading choice due to its capability for centimeter-level localization [8]–[10] and its high resilience to interference [11], [12]. A typical UWB-based RTLS consists of static anchors with known positions and mobile tags whose locations are estimated using techniques such as time difference of arrival (TDOA) or multilateration [13], [14].

Such extensive infrastructure, with anchors requiring wired power connections [13], [14], hinders scalability and impedes economical retrofitting of existing buildings [15]. As already demonstrated commercially for Bluetooth Low Energy (BLE)

(Corresponding author: Silvano Cortesi)

Silvano Cortesi, Lukas Schulthess, Davide Plozza, Christian Vogt and Michele Magno are with the Center for Project-Based Learning, ETH Zürich, 8092 Zürich, Switzerland (e-mail: first-name.lastname@pbl.ee.ethz.ch)

beacon-based indoor navigation, retrofitting is adapted more easily when the anchors or beacons are battery-powered and can operate for multiple years [16]. Therefore, achieving ultra-low power operation is critical for widespread adoption of precise RTLSs, ideally allowing self-sustainable [17] operation to lower installation and maintenance costs. Thus, a key research challenge in realizing practical and large-scale deployments lies in reducing the power consumption of the entire RTLS while maintaining high localization performance [15], [18].

However, conventional radios used for localization, including UWB, are highly inefficient during idle listening, since the transceiver consumes nearly the same amount of power while waiting for potential packets as it does during active communication [19], [20]. This constant energy drain becomes a significant bottleneck in battery-operated mobile systems. To address this issue, ultra-low-power wake-up radios (WuRs) [21], [22], combined with emerging energy-aware algorithms, enable event-driven communication: devices remain in deep sleep, consuming only micro-watts, and activate the main transceiver only upon reception of a dedicated wake-up signal [23].

This approach avoids the fundamental trade-off in traditional RTLS solutions between energy efficiency and responsiveness: Duty cycling or time-scheduled communication schemes can significantly reduce power consumption [24], [25], but they inevitably increase latency, limiting their use in time-critical and event-driven applications [6]. Furthermore, time-scheduling approaches do not account for actual localization needs: when no assets need to be tracked, anchors are still activated regularly to ensure localization, resulting in unnecessary energy consumption [26]. Conversely, continuously active devices allow for low-latency localization; however, they substantially limit the battery lifetime due to the increased energy cost.

While WuR hardware can provide the foundation for on-demand operation, it is the addition of intelligent, energy-aware algorithms that enables a system to strategically manage its resources to maintain long-term energy neutrality [27], [28]. Previous works have shown the theoretical promise of combining UWB and WuRs for achieving accurate and energy-efficient localization, by operating the energy-consuming UWB distance sensing in an event-driven fashion WAKELOC [26], and is detailed as background in Section III-B. In particular, WAKELOC focused on the localization protocol, while ECOTRACK [29] addressed the energy-aware scheduling. By dynamically adapting the sensing and communication rate to the harvested energy, ECOTRACK ensures that devices remain energy-neutral while providing the highest possible amount of global navigation satellite system (GNSS) localizations, thereby balancing performance and battery lifetime in an energy-harvesting deployment.

This work introduces a cooperative and energy-neutral RTLS that integrates ultra-low power WuRs with UWB ranging, addressing the open challenge of enabling sustainable high-accuracy localization despite UWB's inherently high energy consumption. Unlike our earlier studies – WAKELOC, which focused on the localization protocol, and ECOTRACK, which developed adaptive energy-aware scheduling – the pro-

posed approach combines both advances into a unified solution for the more demanding context of UWB-based localization. By fusing ultra-low power wake-up signaling with high-precision UWB ranging, tags and anchors remain in deep sleep until explicitly triggered, while still offering centimeter-level localization accuracy and communication on demand. The system is based on a newly developed sensor node that integrates WAKEMOD [30], together with a DWM3000 UWB transceiver from QORVO and solar energy harvesting capabilities.

In addition, we develop a complete implementation platform that not only realizes the proposed system in hardware but also provides the foundation for experimental validation of its communication primitives and algorithmic intelligence. This platform serves as a proof of concept for sustainable localization, bridging theoretical design with real-world feasibility. The addition of indoor solar harvesting extends this paradigm further by enabling perpetual operation under realistic illumination conditions, thereby reducing maintenance needs and facilitating scalable, long-term deployments. The main contributions of this work are as follows:

- 1) We introduce and evaluate an energy-aware scheduling strategy, aiming to maximize the localization rate of *active* tags by dynamically scheduling ranging opportunities based on energy availability.
- 2) A comprehensive characterization of the system's accuracy across multiple localization solvers and environments, identifying performance trade-offs relevant to real-world deployments.
- 3) To demonstrate system functionality, an open-source¹ ultra-low-power sensor node was developed that integrates WAKEMOD, the DWM3000 UWB transceiver, and solar harvesting. A detailed evaluation of its power consumption and computational cost validates the feasibility of event-driven, high-accuracy localization with self-sustainable operation.
- 4) A real-world deployment utilizing a quadruped robot as a mobile tag, as well as nine anchors, demonstrating practicality in dynamic indoor environments with a localization latency below 83 ms, as well as an open-source simulation framework¹ showing the effects of large-scale deployments.

II. RELATED WORKS

Developing an energy-neutral indoor localization system requires addressing challenges across multiple domains. The following discussion covers UWB-based localization approaches and their scalability limitations, WuR technologies enabling ultra-low-power operation, and positioning algorithms with their computational trade-offs.

A. UWB-Based Indoor Localization Systems

Most three-dimensional localization schemes are based on the capability of UWB to accurately measure distance within centimeter precision [31], [32]. Multiple methods to exploit

¹<https://github.com/ETH-PBL/WakeLoc>

these measurements exist, an overview is presented in this section.

Conventional two-way ranging (TWR) approaches require continuous anchor operation to maintain low-latency localization functionality [26]. Each tag has to exchange multiple messages with at least four anchors, which significantly limits the system's scalability when multiple tags are trying to localize simultaneously [33], [34]. Recent solutions addressed this through scheduling algorithms [35], anchor selection strategies [36], and concurrent transmission techniques [37], [38]. While these approaches improve scalability, the fundamental energy problem of continuous anchor operation remains unsolved.

TDOA-based systems offer better scalability by enabling multiple tags to localize simultaneously from synchronized anchor transmissions [13], [39]. The downlink time difference of arrival (DL-TDOA) approach allows unlimited tag scaling since packet overhead and the resulting complexity of the non-linear systems of equations depend only on the anchor count [40], [41]. However, these systems require complex synchronization infrastructure and coordination between anchors, which limits practical deployment flexibility and introduces scalability issues related to the number of anchors.

Recent hybrid approaches have attempted to combine the benefits of both paradigms. Some systems combine TWR and TDOA to achieve higher accuracy [42], or to facilitate anchor synchronization [34], while others use cooperative positioning where tags share information to improve collective accuracy [14]. However, these approaches still rely on continuously powered infrastructure, preventing truly energy-neutral operation.

Further, Zhang *et al.* [43] explored UWB-based cooperative localization in multi-agent systems, particularly for unmanned aerial vehicle (UAV) clusters, and published a dataset containing all distance measurements between the nodes. They demonstrated cooperative positioning approaches where multiple mobile nodes exploit ranging measurements both to fixed anchors and between themselves, achieving positioning accuracies below 1 m in indoor environments and below 2 m outdoors under various flight formations. Using double-sided two-way ranging (DS-TWR), their approach enables distance-based collaborative navigation without requiring external synchronization infrastructure, though at the cost of increased communication overhead when scaling to larger node counts. While this technique improves robustness, it still requires continuous node operation and does not address long-term energy sustainability.

In this work, we adopt the principle of concurrent transmissions from [37], but in a more relaxed fashion. Our approach allows sequential reception while requiring only a single transmitted message, as shown in WAKELOC [26], thereby targeting both scalability and energy efficiency. Additionally, WAKELOC's passive tags are used to opportunistically exploit the same messages for TDOA [13].

Comparing power consumption with localization quality, UWB transceivers consume over 100 mW during active listening [19], [20], making battery-powered deployments challenging. Duty cycling reduces this issue by introducing latency and

therefore limiting the responsiveness of the localizations [24], [25]. WAKELOC [26] showed that integrating wake-up radios with UWB enables event-driven localization with similar accuracies as [13], [31], but did not address long-term energy neutrality.

B. Wake-up Radio Technologies for Low-Power IoT

WuRs have emerged as a key enabler for event-driven communication in energy-constrained IoT systems [44]. By maintaining ultra-low power listening capabilities while keeping the main radio in deep sleep, WuRs enables systems to achieve both responsiveness and energy efficiency.

Modern WuR architectures achieve listening power consumption in the range of 36 nW to 100 μ W [21], [45], orders of magnitude lower than conventional radio receivers. The sensitivity of WuRs typically ranges from -48 dBm to -75 dBm, with trade-offs between power consumption, reception range, and wake-duration. Recent implementations have demonstrated successful integration with various main radio technologies, including BLE [46], and UWB [30].

A specialized WuR integrated circuit (IC) is the FH101RF from FRAUNHOFER, used in WAKEMOD [30]. It is the only commercially available WuR, offering tri-band reception (433 MHz, 868 MHz and 2.4 GHz), idle listening consumption of 6.9 μ W and a sensitivity of -72.6 dBm whilst achieving wake-up latencies below 55 ms – placing it close to state-of-the-art ICs from academia [21], [47], while keeping commercial availability and flexibility.

In our work, we exploit these advances by integrating WAKEMOD with its commercially available WuR into a UWB localization system, demonstrating that energy-neutral operation is feasible not only in theory but with practical, off-the-shelf components.

C. Positioning Algorithms and Computational Trade-offs

The choice of a three-dimensional positioning algorithm from known anchor positions has a significant impact on both localization accuracy and computational energy consumption, particularly for resource-constrained devices operating under strict energy budgets.

For multilateration problems, optimal solutions exist through eigenvalue decomposition approaches [48], [49]. These methods achieve the statistically minimal error for given range measurements but require an eigendecomposition of a sparse matrix. In their comparison with state-of-the-art solvers [50]–[52], Larsson *et. al.* showed the highest accuracy with 34 cm in average over eight datasets, with the average solver having an error of 70 cm. In terms of runtime complexity, it is $47 \times$ more efficient than the average of the other solvers, and only 16 % slower than the fastest solver [51].

Iterative methods, particularly the Levenberg–Marquardt (LM) algorithm [53], [54], offer a practical alternative with reduced computational requirements. While not guaranteed to find the optimum, LM-iteration typically converges quickly for well-conditioned localization problems and can be implemented with limited memory usage. The trade-off between

solution quality and computational cost makes iterative approaches interesting for energy-constrained systems.

In addition to the above methods, TDOA positioning presents additional algorithmic challenges due to the hyperbolic nature of the constraint equations [40], [41]. Closed-form solutions exist for specific geometric configurations, but general cases require iterative or particle filter-based non-linear least squares solvers [41].

We address these challenges by tailoring TDOA and multilateration solvers to operate within the limited energy and computational resources of our platform, enabling scalable cooperative localization without sacrificing feasibility.

III. SYSTEM ARCHITECTURE AND CHARACTERIZATION

The proposed localization system described in this section consists of the anchor and tags, as shown in Fig. 1, a localization protocol based on WuRs and being processed online on the tags wanting to localize, and an energy-aware localization-scheduling algorithm.

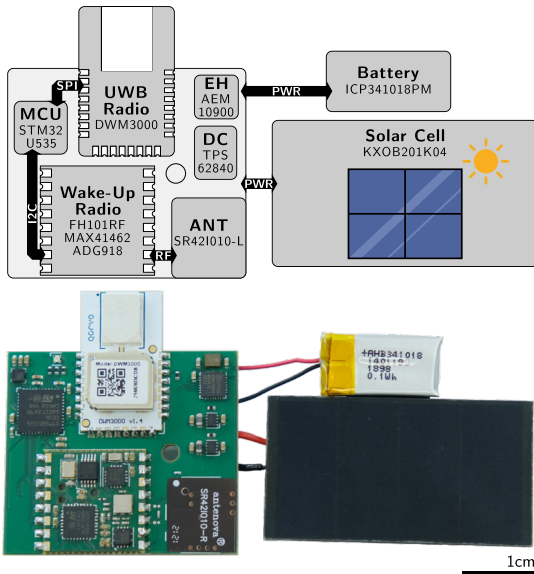


Fig. 1. Overview of the developed sensor node used for anchors and tags.

A. Hardware design

The hardware architecture is based on energy harvesting from a solar cell, combined with a small lithium-polymer (LiPo) battery for buffering, ensuring autonomous operation. It combines an UWB transceiver for localization with the WAKEMOD WuR for efficient idle listening, all managed by a low-power microcontroller (MCU).

The energy harvesting capability is based on an EPEAS AEM10900 boost converter with integrated maximum power-point tracking (MPPT) tracking. An ANYSOLAR KXOB201K04TF solar cell with a size of 23 mm × 42 mm is used as energy source. The cell is selected with an open-loop voltage close to the harvesters' maximum input voltage, at which point it achieves its highest efficiency. A 35 mAh LiPo battery is used to buffer energy during low-light conditions.

The 1.8 V supply of the node itself is generated using the high-efficiency 60 nA-quiescent current buck converter TPS62840 from TEXAS INSTRUMENTS.

The STMICROELECTRONICS STM32U535CEUX microcontroller is based on a ARM CORTEX-M33 with floating point unit (FPU), operates at frequencies up to 160 MHz, and is equipped with 512 kB of flash memory and 274 kB of SRAM. It has a power consumption of $16.3 \frac{\mu\text{A}}{\text{MHz}}$ and permits a low-power state of 90 nA in shutdown mode.

Localization is carried out with the QORVO DWM3000 UWB module, achieving a low power consumption around 230 nA in deep sleep. The configurations of the UWB transceiver using [55] are optimized to achieve high range (channel 5) while maintaining low TX consumption (128 bit preamble).

The final building block is the WuR module WAKEMOD [30]. The open-source module is designed around the FRAUNHOFER FH101RF WuR radio and the ANALOG DEVICES MAX41462 amplitude shift-keying (ASK) transmitter, both connected through an ANALOG DEVICES ADG918 radio frequency (RF) switch to the same antenna. The module designed for 868 MHz, achieves a reception sensitivity of -72.6 dBm and a transmission power of up to 2.78 dBm at 1.8 V. With its consumption of $6.9 \mu\text{W}$ when actively listening, the system remains in deep sleep and only wakes up upon receiving a wake-up call (WuC).

B. Localization Protocol and Algorithms

The employed localization method is based on WAKELOC [26]. Tags can obtain their position either by *actively* initiating a localization procedure themselves (*active* mode) or by *passively* reusing the messages exchanged during another tag's localization procedure (*passive* mode) – making it scalable in the amount of tags being part of the RTLS. An overview of this scheme is illustrated in Fig. 2.

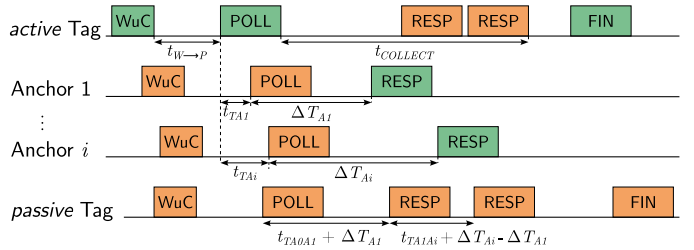


Fig. 2. WAKELOC localization scheme as shown in [26], combining TWR with TDOA. Messages in green are transmissions, orange represents receptions.

In *active*-mode, a tag first wakes nearby anchors with a WuC and then performs multilateration based on a nested carrier frequency offset corrected single-sided two-way ranging (CC-SS-TWR) exchange. Compared to naive approaches, this nested scheme reduces the number of required messages to $N_A + 1$ for a localization with N_A anchors. The tag computes its own position from the collected distance measurements and finally broadcasts its estimate.

The delay ΔT_{Ai} of each anchor's response depends on its index, using $\Delta T_{Ai} = \Delta T_{fix} + \Delta T \cdot [(i - 1) \bmod \hat{N}_A]$ to

ensure scalability. The value of \hat{N}_A is chosen such that no two anchors within reception range reply simultaneously, requiring some spatial separation in their placement.

In *passive*-mode, a tag reuses the localization exchange triggered by an *active* tag. After receiving the initial WuC, it listens for the poll and response messages of nearby anchors and applies TDOA to derive its position. The missing information, namely the position of the *active* tag, is obtained from the *active* tag's final broadcast.

With this combination of TWR and DL-TDOA, WAKELOC achieves scalability for both the number of anchors and tags, whose low latency only depends on the WuR, and allows for ultra-low power consumption on the anchors while they are actively listening. However, the tag performing *active* localization consumes more energy than in a standard TWR system, as it additionally needs to transmit the WuC and broadcast its position.

For localization, the tag acting as the *active* one must execute its localization through multilateration, whilst a tag acting *passively* applies TDOA. Larsson *et al.* [48] proved that the multilateration problem can be converted to an eigenvalue problem and thus be solved optimally (if the eigenvalues can be found exactly), achieving the statistically minimal error with the available measurements. Next to Larsson, the LM-iteration [53], [54] was evaluated from the class of iterative (though non-optimal) solvers.

The TDOA problem of the *passive* tag, again a non-linear least squares problem, is solved as well using LM-iteration. The different solvers implemented in this work are made available as an open-source library on GITHUB².

C. Energy-Aware AIMD Algorithm

The energy-aware and cooperative algorithm closely builds on ECOTRACK [29]. The algorithm is based on the principle of dynamically adapting the number of *active* localizations according to the available harvested energy, with the battery state of charge serving as a proxy for energy income. The approach follows the additive-increase/multiplicative-decrease (AIMD) paradigm, well known from congestion control in computer networks. The algorithm increases the hourly localization rate linearly by one, as long as sufficient energy is available, but halves the rate (multiplicative decrease with factor 2) once the battery indicates a lack of energy. The transitions between these states are controlled by a finite state machine (FSM) in combination with a metric function.

1) *Finite state machine (FSM)*: The FSM of ECOTRACK, illustrated in Fig. 3, operates on the variable k , defined as the number of *active* localizations per hour (of the tag running this instance of the FSM): It either holds k , increments k by one, or halves k .

State transitions are triggered by evaluating ECOTRACK's metric function m against two thresholds β_1 and β_2 , which determine whether the tag should increase or decrease the *active* localization rate. In addition, a battery-level threshold γ ensures that the algorithm always increases k whenever the

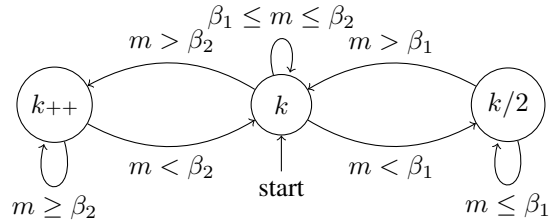


Fig. 3. State diagram of the FSM-based adaptive sampling algorithm: $k/2$ means that k halves in the next step; $k++$ means that k increases by a fixed rate in the next step, in our case by one; k means that k stays the same in the next step.

state of charge is high enough. Together, β_1 , β_2 and γ represent the tunable parameters of the FSM.

2) *Metric Function*: The ECOTRACK's metric function m is defined in Eq. (1). It evaluates the change in battery state $b[t]$ between consecutive hours, normalized by the battery capacity B . The metric is rewarded when the battery state is high or increasing, and penalized when the state is low or decreasing. In particular, when the battery charge remains above the boundary γ , the algorithm always increases the localization rate, whereas a decrease in battery state triggers a multiplicative decrease of k . This mechanism allows the system to adapt smoothly to fluctuating energy availability, maximizing the number of *active* localizations while preserving long-term sustainability.

$$m = \underbrace{B \cdot (b[t] - b[t-1])}_{\text{batt. state difference}} - \underbrace{\left(\frac{1}{b[t]} - 1 \right)}_{\text{low batt. penalty}} + \underbrace{\begin{cases} \infty, & \text{if } b[t] \geq \gamma \\ 0, & \text{otherwise} \end{cases}}_{\text{high batt. reward}} \quad (1)$$

A second version of this metric (Eq. (2)) keeps an upper bound on the number of *active* localizations per day (system constraint, *not* tuned), bounding the rate once this limit is reached.

$$m_{\text{bounded}} = \underbrace{\begin{cases} m, & \text{if } k < k_{\max} \\ \min \left(m, \frac{\beta_1 + \beta_2}{2} \right), & \text{otherwise} \end{cases}}_{\text{bound on max. localizations}} \quad (2)$$

3) *Algorithm Tuning*: The parameters β_1 , β_2 and γ are tuned off-line and globally to optimize performance subject to the constraints in Eq. (3). For each tag j , the battery state at the end of the year must be at least 10 %. During tuning, all batteries are initialized at 10 % state-of-charge (SoC) to model a conservative starting condition.

$$\begin{aligned} b_j[T] &\geq 10\% \quad \forall j \\ b_j[\cdot] &\leq 100\% \quad \forall j \end{aligned} \quad (3)$$

The optimization problem in Eq. (4) is formulated to maximize the mean number of *active* and *passive* localizations across all tags over one year. Let $l_j[t] \in \mathbb{N}$ denote the number of localizations of tag j on day t . Then,

$$J = \max_{\{l_n[t]\}} \left(\frac{1}{N_T} \sum_{j=1}^{N_T} \sum_{t=1}^T l_j[t] \right) \quad \text{subj. to Eq. (3)} \quad (4)$$

²<https://github.com/ETH-PBL/WakeLoc-Algorithm>

where N_T is the number of tags and T the number of days in the year.

Each tag then schedules every hour the *active* localizations for the next hour in a uniformly at random manner, thereby improving temporal coverage. Furthermore, the algorithm regulates only *active* localization decisions. In simulation, *passive* localizations are always performed opportunistically, whenever energy is available, enabling tags to exploit ongoing communication exchanges and making the algorithm intrinsically cooperative.

IV. EXPERIMENTAL SETUP

To validate the system's performance and accuracy, several evaluations were conducted targeting four core aspects: localization accuracy across different solvers, performance and power consumption of the ultra-low-power sensor node, and system behavior in both controlled and real-world deployments, including quadruped-robot evaluation and large-scale simulation. The following subsections describe each experimental setup in detail.

A. Localization Accuracy

In order to evaluate the different algorithmic solvers for localization (Larsson and LM-iteration for multilateration and LM-iteration for TDOA as described in Section III-B), an experiment was set up in a room measuring $8.6 \text{ m} \times 7.6 \text{ m}$. A BOSCH GLM150-27C laser distance meter and a VICON motion capture system were employed to provide the ground truth.

To minimize the geometric dilution of precision (GDOP), five anchors were strategically positioned on the given infrastructure to attain optimal spatial coverage [10], [56] (GDOP of 0.090). Two tags, one *active* and one *passive*, were placed at varying heights within a $5 \text{ m} \times 5 \text{ m}$ grid. A total of 200 distinct positional combinations were tested. For this, first the *active* tag was moved on the grid with the *passive* fixed in position, and then vice versa. Around 480 distinct measurements were conducted for each position combination, yielding a dataset of 95 457 measurements. A first preliminary measurement of each anchor was employed to calibrate its antenna delay. The measurement setup is shown in Fig. 4.

In a second evaluation, the RTLS has been evaluated in a realistic scenario as depicted in Fig. 7. The experimental setup included an office with a size of $5.7 \text{ m} \times 7.0 \text{ m}$ and an adjacent corridor of size $3.8 \text{ m} \times 14.7 \text{ m}$, with a total space of 91 m^2 . In this real-world use case, the tags were mounted on the top of a UNITREE A1 quadruped robot equipped with the sensor backpack described in [57]. An *active* tag and a *passive* tag were positioned at a height of 53.4 cm from the ground and separated by 20.7 cm. The experiment involved the robot leaving the office and traversing the corridor. A total of nine anchors and two tags were deployed in this setup. The robot's HOKUYO UTM-30LX-EW 2D LiDAR with Adaptive Monte Carlo Localization (AMCL) as described in [57] was used as ground truth, as its centimeter-level accuracy exceeds the precision required to benchmark the RTLS.

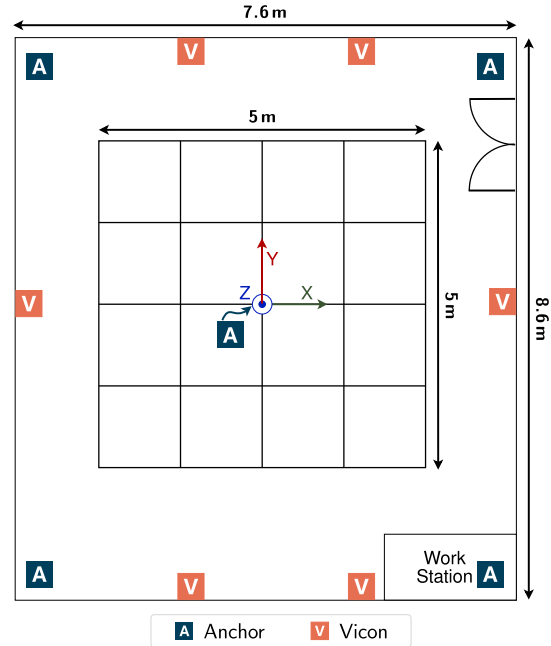


Fig. 4. Experimental setup for evaluating the localization accuracy. A represents anchors, V the cameras of the VICON system.

B. Computational Cost

The recorded dataset collected as described in Section IV-A was used to evaluate the three microcontroller implementations (optimal/iterative multilateration, iterative TDOA) on the MCU. In addition, four distinct solver tolerances (10^{-2} , 10^{-4} , 10^{-6} , and 10^{-8}) were used during evaluation. On the LM algorithms, the tolerance is used as the relative tolerance for early stopping the iteration, whereas on the Larsson algorithm, it is used inside the inverse iteration during eigenvector calculation. This approach allows for a quantitative examination of both localization statistical accuracy (mean error, variance) and algorithmic performance (computational time, resource demands) - both evaluated on the developed sensor node. The computation time was measured using the Data Watchpoint and Trace (DWT) peripheral of the ARM CORTEX-M33 MCU.

Three scenarios were evaluated for the LM-TDOA solver: *i*) Assuming the known position of the *active* tag (classical TDOA), *ii*) using the position of the *active* tag estimated by the Larsson multilateration, and *iii*) using LM multilateration.

C. Power Consumption

The power consumption of the nodes was analyzed using a KEYSIGHT N6705C DC Power analyzer fitted with three N6781A source measurement units. Three nodes have been attached to the power analyzer simultaneously on three different channels, one configured as an anchor, the others as *active* and *passive* tags respectively. Using a sampling frequency of 48.8 kHz, power profiles of the three nodes were recorded over a 30 s window and multiple localizations.

D. Energy-Aware Simulation-Based Evaluation

Next to the real-world deployment, we created a simulation framework to estimate the behavior of a large-scale deploy-

ment with respect to the proposed energy-aware localization algorithm.

Geometrically, the simulation is based on the DEPT environment of the CLOVES testbed [58], covering an area of 6382 m² consisting of two larger open spaces connected by a narrow corridor. The deployment includes 89 anchor positions. In addition, scenarios with 5, 20, and 100 randomly placed tags were simulated over one year. For a successful localization, a minimum of five successful anchor responses was assumed.

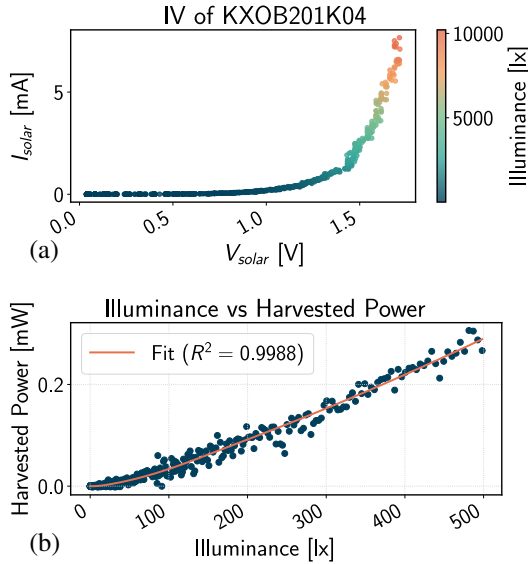


Fig. 5. Solar cell and harvester characteristics. (a) shows the IV-curve of the KXOB201K04 solar cell, and (b) shows the measured relation between light intensity and harvested power into a 3.7 V sink together with a fitted polynomial function.

As no long-term dataset was available for our specific harvester and solar cell, the indoor solar harvesting dataset presented in [59] was used, providing over two years of indoor solar harvesting measurements from six different locations inside an office building. At each location, the illuminance was recorded at a frequency of 1 Hz. For the purpose of this evaluation, the complete year 2018 was considered with its five monitored positions. These locations represent a wide range of lighting conditions, from window-facing offices to hallways with very little natural light.

To adapt the dataset to our sensor node electronics, first, the AEM10900 together with the KXOB201K04 solar panel was characterized in a solar testbed connected to two KEYSIGHT B2902A source-measurement units. The relation was measured across 1000 illuminance levels from 0.2 lx up to 10 klx at a MPPT of 75 %, as shown in Fig. 5.

Three sigmoid-blended polynomials were fitted to the measured data for the regions 0.2 lx–15 lx, 15 lx–1500 lx, and 1500 lx–10 klx. The resulting illuminance-to-harvested-power model achieved an R^2 of 0.9988. Using this model, the illuminance measurements from Sigrist *et al.* [59] datasets were transformed into the power harvestable by our system and downsampled to one sample per minute. The daily harvestable energy ranges from only 0.31 ± 0.13 J in dim environments to up to 18.51 ± 20.65 J in bright settings, with typical indoor conditions giving about 1.81 ± 1.21 J per day.

Based on these considerations, the simulation was set up as follows: each anchor and tag was equipped with an empty 35 mAh battery in the simulation (charged to 0 %), as well as a randomly assigned energy harvesting profile from the dataset. Battery self-discharge was modeled according to the RENATA userguide [60]: 4 μ A leakage at full capacity and 1 μ A at 30 % SoC, interpolated linearly in between.

At every simulation step (one minute), first, every node received harvested energy corresponding to its harvesting profile. Then, tags were processed in randomized order to ensure fairness for their energy-aware algorithm. For each tag, the decision to initiate *active* localization was made using the algorithms introduced in Section III-C. Both strategies were compared to a constant-rate algorithm (with the rate being a tunable parameter), where each tag tries to perform a static amount of *active* localizations per hour. For both the AIMD-based and constant-rate algorithms, the parameters were tuned only at the average-light positions P06 and P13 prior to the full-year simulations and in a simulation with 100 randomly and uniformly distributed tags in the simulation environment. The limit for the constant-rate algorithm to fulfill the constraints in Eq. (3) is one *active* localization per hour. The bound for the bounded-AIMD is set to 6 localizations per hour.

If a tag decides to perform an *active* localization, anchors within 20 m line-of-sight (LOS) or 5 m non-line-of-sight (NLOS) will be considered. The number of anchors within reach of each other \hat{N}_A has been set to 10. Each anchor's energy is reduced according to the power characterization presented in Section V-C. A response is considered successful only if the anchor's battery remained non-empty afterwards. If at least five anchors respond successfully, the localization is considered successful; otherwise, the attempt is considered a failure. Neighboring tags within the range of the same anchors are able to perform *passive* localization in the same timestep. If more than five successful anchor responses are observed, the *passive* localization succeeds. Finally, the tag's battery state

TABLE I
ACCURACY RESULTS DEPENDING ON THE LOCALIZATION TYPE AND USED ALGORITHM. VALUES ARE GIVEN IN cm.

	WAKELOC <i>active</i> (TWR)		WAKELOC <i>passive</i> (TDOA)		
	Larsson	LM	TDOA with GT	TDOA with Larsson	TDOA with LM
avg	21.68 cm	21.89 cm	33.05 cm	25.66 cm	25.70 cm
md	16.13 cm	16.13 cm	27.49 cm	19.81 cm	19.86 cm
$\sigma(\cdot)$	17.02 cm	17.13 cm	24.84 cm	18.97 cm	19.05 cm
min $\ \cdot\ $	0.28 cm	0.27 cm	0.35 cm	0.42 cm	0.26 cm
max $\ \cdot\ $	497.72 cm	345.75 cm	485.79 cm	464.38 cm	469.36 cm

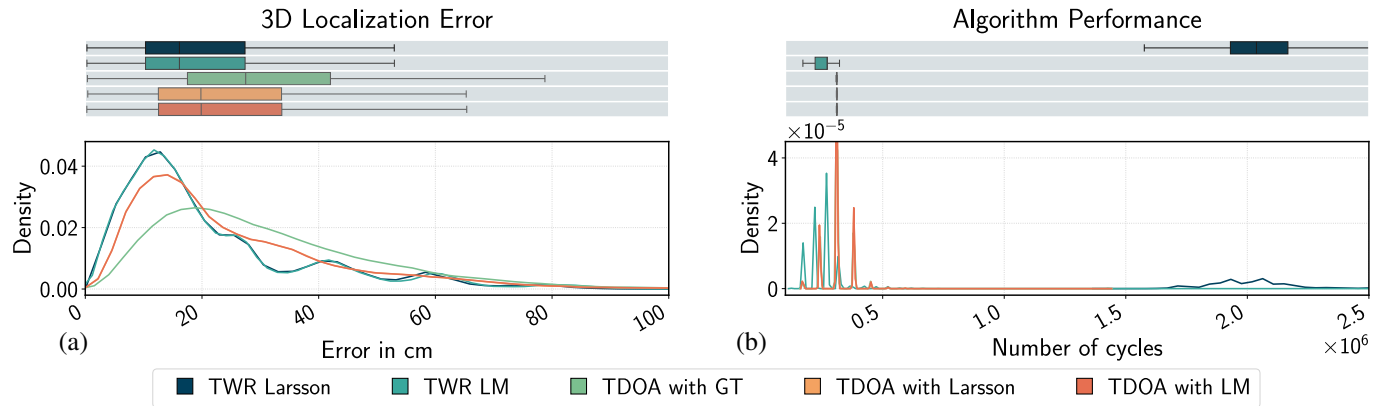


Fig. 6. Localization accuracy (a) and computational cost (b) of different multilateration and TDOA solvers.

was adjusted accordingly to the consumption.

V. RESULTS

Using the results obtained through the measurements as described in Section IV, this section presents their results and discusses their findings. The evaluations contains both controlled and real-world deployments, providing comprehensive validation of the system's capabilities. The following subsections detail the results for localization accuracy, computational performance, power consumption characteristics, and large-scale energy-aware and cooperative behavior.

A. Localization Accuracy

The resulting position results obtained using the measurements described in Section IV-A were almost identical across all tolerances (sub-mm changes) and are summarized in Table I for a solver tolerance of 10^{-2} and shown in Fig. 6. It can be seen that the maximum error for the multilateration with the LM-iteration is lower, while the average error of 21.89 cm is slightly higher than with the Larsson algorithm (21.68 cm on average, median 16.13 cm). For the TDOA solver, utilizing the active tag's position estimated via multilateration yields higher localization accuracy than relying on the initiator's ground truth. While classic TDOA based on the ground truth resulted in an average error of 33.05 cm, employing multilateration estimates from the Larsson algorithm and the LM-iteration improved the accuracy to 25.66 cm and 25.70 cm, respectively. This phenomenon aligns with observations made in [26], which attribute such performance gains to the availability of additional measurement data.

These results highlight two important points: First, the Larsson algorithm performs marginally better on average than the LM-iteration, consistent with its theoretical property of solving for the optimum. In rare cases, however, the LM-iteration achieves better convergence, as evidenced by its smaller maximum error. The large maximum error for the Larsson algorithm occurred when it failed to converge within 1000 power method iterations (427 ms), unable to properly solve for the maximum eigenvalue. This convergence failure can occur when iteratively solving for the eigenvalues in poorly conditioned scenarios, particularly when sensor geometry is unfavorable or when significant measurement noise is present [61], [62]. Second, there is a negligible difference in the TDOA results when using either multilateration method, as also seen in Fig. 6 where the curves for "TDOA with LM" and "TDOA with Larsson" almost perfectly overlap.

The evaluation in a real-world scenario on the quadruped robot (see Fig. 7 and Table II) shows slightly poorer results. On the one hand, the anchors are not optimally placed in terms of their GDOP. On the other hand, anchors for which there is no direct LOS are also taken into account in the position determination – even though these could in a further step be excluded by using the UWB messages' channel-impulse response (CIR). The crossed-out position estimates are recognized by the localization algorithm as either due to a lack of convergence or an insufficient number of available anchors (< 4) and classified as outliers.

The results of the *active* tags continue to show that the Larsson algorithm and the LM-iteration provide comparable accuracy, with average deviations of 43 cm (both without taking into account the estimates identified as outliers). No-

TABLE II
REAL-WORLD EVALUATION OF THE ACCURACY AGAINST THE LIGHT DETECTION AND RANGING (LiDAR) OF THE QUADRUPED ROBOT. VALUES ARE GIVEN IN m.

	WAKELOC <i>active</i> (TWR)				WAKELOC <i>passive</i> (TDOA)			
	Larsson		LM		TDOA with Larsson		TDOA with LM	
	w outliers	w/o outliers	w outliers	w/o outliers	w outliers	w/o outliers	w outliers	w/o outliers
avg	0.47 m	0.43 m	0.48 m	0.43 m	6.81 m	4.03 m	5.76 m	6.91 m
md	0.34 m	0.37 m	0.36 m	0.35 m	0.46 m	0.43 m	0.52 m	0.46 m
$\sigma(\cdot)$	0.49 m	0.25 m	0.35 m	0.24 m	16.64 m	10.59 m	15.18 m	16.83 m
min $\ \cdot\ $	0.05 m	0.08 m	0.05 m	0.06 m	0.04 m	0.04 m	0.03 m	0.03 m
max $\ \cdot\ $	4.07 m	1.31 m	2.02 m	1.27 m	107.33 m	64.74 m	68.81 m	68.81 m

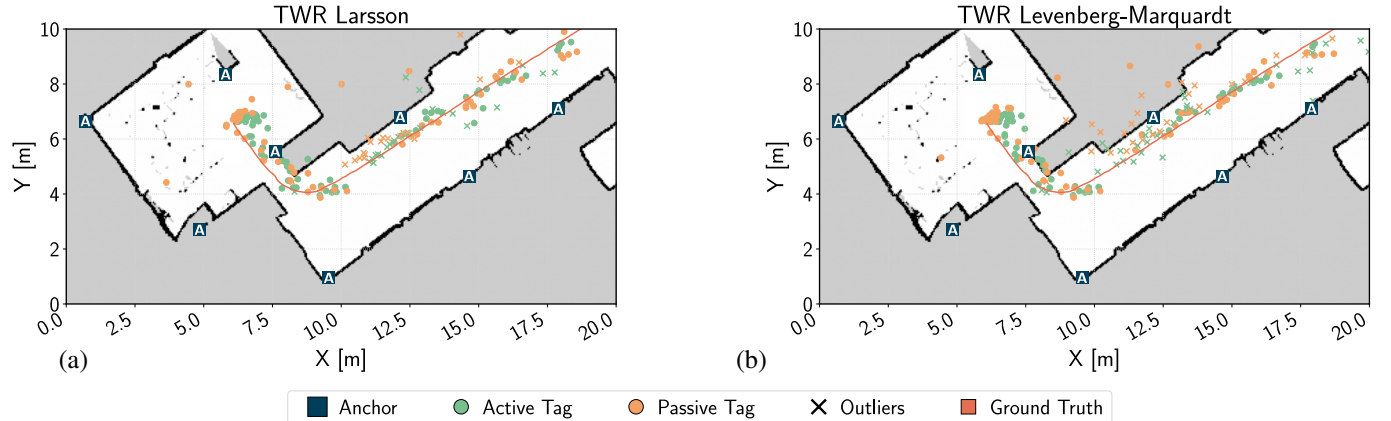


Fig. 7. Localization of a dynamic object in a real-world environment. (a) shows the results when using Larsson's multilateration method, (b) when using LM-iteration. Outliers are marked where localization failed due to having very few anchors (three or fewer) or a lack of convergence within 20 iterations.

tabley, the LM-iteration has a lower variance due to occasional convergence failures of the Larsson algorithm, resulting in smaller maximum errors (2.02 m versus 4.07 m). The results of the *passive* tags suffer significantly from the less accurate position determinations of the *active* tags and from the NLOS conditions – an effect that has already been demonstrated in [63]. While the median accuracy reaches up to 0.46 m, the average and, in particular, the maximum errors are significantly higher. With knowledge of the building plan, these errors could be detected and reduced.

B. Computational Cost and Performance

The results in this section are based on the measurements described in Section IV-B. For all solver tolerances, the average number of MCU cycles varied by about 15 %, between a tolerance of 10^{-2} and one of 10^{-8} . It is therefore notable that convergence with the iterative solvers – if it succeeds – happens quickly, which can be observed due to the minimal changes in the estimation errors across different solver tolerances. Here, it is important to distinguish between the number of algorithm iterations required for convergence and the resulting number of cycles. The average number of iterations (for both multilateration, as well as TDOA) the Levenberg–Marquardt solver took to converge is four iterations. A cut-off at 20 iterations is used to identify non-converging cases. When multilaterating, non-convergence occurred in 8 out of 95 457 cases for both the LM-iteration and the Larsson algorithm. In TDOA, non-convergence occurred in 96 cases

when using ground truth data of the *active* tag, 97 when using the estimate, respectively.

The computational cost of the different algorithms is listed in Table III and Fig. 6b). The Larsson algorithm requires, on average, 2 156 437 clock cycles. The LM-based multilateration takes 267 244 cycles. For TDOA, the LM-based solver of the *passive* tag takes about 312 427 cycles on average. In Fig. 6b), one can clearly see the individual iterations of the iteration-based solvers.

C. Power Consumption

The power consumption of the anchors and tags (one acting as an *active* tag, one as a *passive* tag) in deep sleep, with the WuR actively listening, is $7.84 \mu\text{W} - 1.15 \mu\text{W}$ higher than the consumption of the WAKEMOD alone.

Table IV shows a breakdown of the energy consumption of the sensor nodes during a localization cycle, broken down by device type and localization method. *Active* tags consume the most energy at 3.22 mJ per localization, as they actively transmit the WuC and initiate measurements. *Passive* tags require significantly less energy (951.16 μJ), as they only receive and process signals from *active* tags. The consumption of the anchors depends on the anchors' node number: Each localization causes $338.30 \mu\text{J}$ of basic energy plus $15.28 \mu\text{J}$ per localization, bound by \hat{N}_A as described in Section III-B.

The duration of the localization dictates the latency as well as the maximal localization rate. With a duration and latency of 84.52 ms, the maximal localization frequency is 11.8 Hz.

TABLE III

COMPUTATIONAL EVALUATION DEPENDING ON THE LOCALIZATION TYPE AND USED ALGORITHM. VALUES ARE GIVEN IN CYCLES AND ms. FOR READABILITY, THE TABLE LISTS EXECUTION TIME IN ms, DERIVED FROM THE 144 MHz MCU CLOCK.

WAKELOC <i>active</i> (TWR)					WAKELOC <i>passive</i> (TDOA)					
Larsson			LM		TDOA with GT		TDOA with Larsson		TDOA with LM	
avg	2 156 437	14.98 ms	267 244	1.86 ms	317 035	2.20 ms	312 427	2.17 ms	312 445	2.17 ms
md	2 037 673	14.15 ms	271 548	1.89 ms	311 197	2.16 ms	311 630	2.16 ms	311 630	2.16 ms
$\sigma(\cdot)$	777 012	5.40 ms	67 046	0.47 ms	70 249	0.49 ms	54 194	0.38 ms	54 194	0.38 ms
min $\ \cdot\ $	1 435 471	9.97 ms	122 750	0.85 ms	170 021	1.18 ms	170 902	1.19 ms	170 900	1.19 ms
max $\ \cdot\ $	61 419 270	426.52 ms	2 495 594	17.33 ms	1 434 213	9.96 ms	1 432 733	9.95 ms	1 433 041	9.95 ms

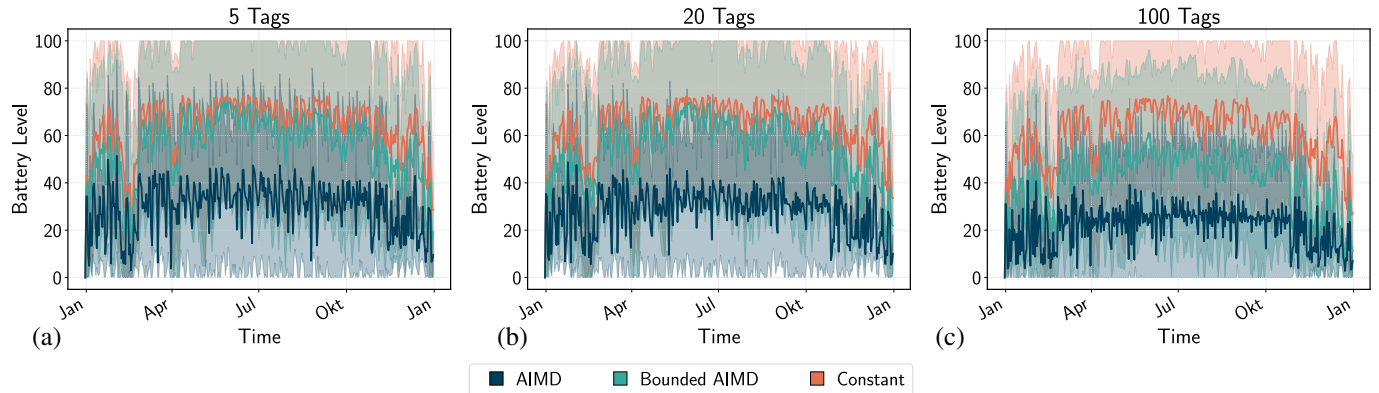


Fig. 8. Average tag battery SoC over the simulated year for simulations with (a) 5, (b) 20, or (c) 100 tags. Shaded area shows the standard deviation.

TABLE IV

BREAKDOWN OF THE SENSOR NODES' POWER CONSUMPTION.

	active Tag	passive Tag	Anchor
Local.	Energy	3.22 mJ	951.16 μ J
	Duration	84.52 ms	$338.30 \mu\text{J} + 15.28 \mu\text{J} \cdot [(i-1) \bmod \hat{N}_A]$ $30.55 \text{ ms} + 290 \mu\text{s} \cdot [(i-1) \bmod \hat{N}_A]$
Sleep	Power	7.84 μW	7.84 μW

D. Energy-Aware Simulation

The evaluation of the simulation focused on the achievable total number of localizations per tag and day, as well as the SoC of the battery over the year.

The results in Fig. 8 show the average SoC of the tags over the entire simulation period. Regardless of the algorithm selected and the network size, the tags achieved to maintain an average charge of 7% at the end of the simulated year. The AIMD consumed most energy, followed by the bounded-AIMD and the constant rate algorithm. Notably, the AIMD had the smallest standard deviation over the year, showing that it adapts very well to different light conditions.

Furthermore, as the number of tags *actively* locating increases, the energy consumption of all tags rises because more *passive* localizations take place. However, this effect remains small for two reasons: *i*) *active* localization consumes about three times as much energy as *passive* localization, and *ii*) most of the additional *active* localizations - especially under the AIMD variants, happen during conditions with a higher energy

supply.

Anchors maintain a higher SoC than tags, reflecting their lower activity and energy consumption. For tags and anchors operating under the low light harvesting profile, the AIMD-based algorithm detects the declining battery state according to the metric in Eq. (1) and reduces the *active* localization rate to zero. At this point, the devices remain in their lowest sleep state, listening only on the WuR. However, even this minimal power consumption cannot be sustained, as the average harvested power of $3.59 \mu\text{W}$ is not sufficient to maintain even the sleep consumption and self-discharge of the battery. Consequently, all tags and anchors that operated under this lighting profile had completely discharged their batteries already very early in the year.

For anchors, the median SoC at the end of the year is between 30% to 40% across all tested algorithms and network sizes. However, the choice of rate-control algorithm affects how often anchors end up with a low battery (0% to 25% SoC): with AIMD, all anchors fall in this category, while bounded-AIMD and constant rate reduce it to about 60% and 50%, respectively. Increasing the number of tags has only a moderate effect on anchors. Their average SoC ranges from 29% (with AIMD) and 39% (constant-rate), showing how WAKELOC effectively stabilizes anchor consumption even as the number of tags scales up.

Fig. 9 shows the average number of localizations per day and per tag for the three simulated network sizes (5, 20, and 100 tags). The AIMD and bounded-AIMD algorithms perform significantly more localizations than the constant-rate

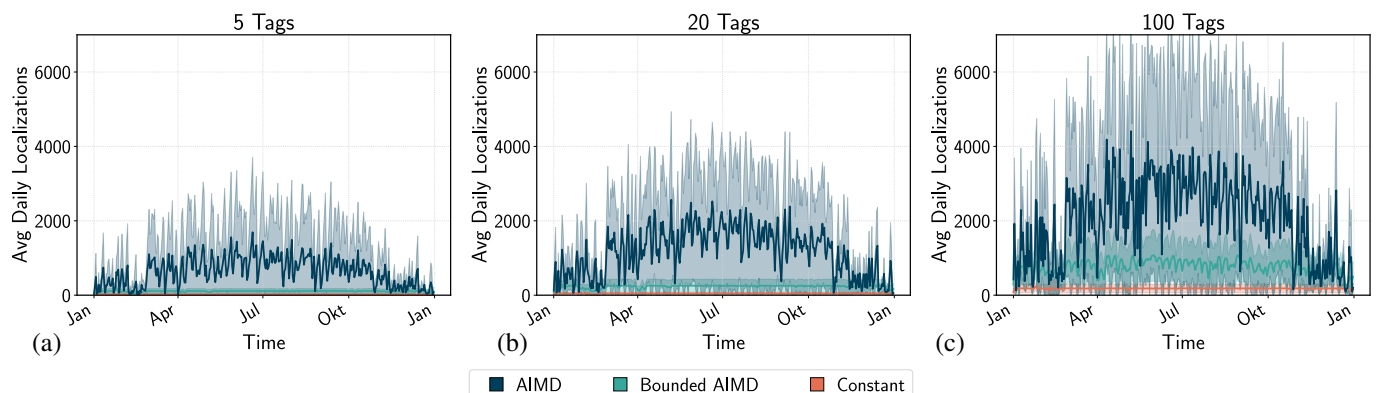


Fig. 9. Average localizations per day and tag for simulations with (a) 5, (b) 20, or (c) 100 tags. Shaded area shows the standard deviation.

TABLE V
STATISTICS OF THE LOCALIZATIONS PER DAY OF TAGS AND ANCHORS.

# Tags	AIMD			Bounded AIMD			Constant Rate		
	5 T, A	20 T, A	100 T, A	5 T, A	20 T, A	100 T, A	5 T, A	20 T, A	100 T, A
avg	634, 199	1173, 1056	2031, 2554	105, 35	234, 186	761, 811	19, 7	42, 34	180, 182
md	154, 0	569, 274	1092, 1814	141, 0	281, 142	805, 848	24, 0	48, 24	193, 184
$\sigma(\cdot)$	886, 568	1375, 1397	2398, 2564	60, 74	167, 168	550, 568	10, 26	29, 38	123, 140
min	0, 0	0, 0	0, 0	0, 0	0, 0	0, 0	0, 0	0, 0	0, 0
max	4211, 4232	6194, 7935	14354, 14341	295, 1681	576, 1739	3108, 5899	67, 1281	96, 1250	2807, 3083

algorithm. Especially, this increased activity occurs mainly during the summer months, when above-average amounts of light and thus energy are available. On the strongest days in July, the AIMD algorithm achieves up to an average of 2400 localizations per day and tag in the 100 tags deployment, while the constant-rate algorithm remains constant at around 180 localizations (*active* and *passive* combined).

Table V summarizes the statistical parameters of the localizations. For all network sizes, AIMD enables the most localizations on average (up to 2031/2554 for tags/anchors), followed by bounded-AIMD (761/811) and constant-rate (180/182). The standard deviations also indicate that the number of localizations depends heavily on daylight availability, which is particularly visible in large networks. Minima of 0 indicate that the tags and anchors without energy were unable to perform localization. Maxima of over 13 000 localizations with 100 tags demonstrate the scalability of the AIMD approach in times of high energy availability – always trying to make best use of the available energy. In addition, the distribution of localizations shows that AIMD and bounded-AIMD respond particularly well to seasonal variation: they make efficient use of phases with plenty of light, while constant-rate remains constant and does not adjust resources. This confirms the advantages of energy-adaptive algorithms, especially in heterogeneous lighting environments where some tags have significantly more energy available than others.

The bounded-AIMD algorithm, while achieving a lower average localization rate compared to AIMD, shows an advantage during periods of very low light intensity. By conserving energy more aggressively, bounded-AIMD maintains higher battery levels, enabling nodes to sustain higher localization rates under scarce energy availability. In contrast, the standard AIMD drastically reduces its localization rate in such scenarios, resulting in fewer successful localizations when energy input is minimal.

Summarizing, the AIMD achieved in average a $2.7 \times$ to $6.1 \times$ higher localization rate per day and tag than bounded-AIMD, and a $11.3 \times$ to $33.7 \times$ higher rate than the constant rate algorithm. At the same time, the battery SoC at the end of the year was only $1.6 \times$ to $2.2 \times$, and $2.9 \times$ to $3.9 \times$, lower for the tags, respectively. Together, these numbers demonstrate that energy-aware algorithms can significantly improve the localization rate of the whole network, without compromising too much on the battery and almost fulfilling the same design constraints of maintaining an average charge of 7% at the end of the year.

Even though the algorithm parameters were tuned under average-light conditions, the scheme scaled well to nodes under more high-light illumination as well: none of the tags or anchors remained with a battery state above 75% at the end of the year, indicating efficient utilization of available energy across heterogeneous light conditions.

VI. CONCLUSION

This work presents ECO-WAKELOC, a scalable and energy-neutral UWB indoor localization system that addresses the fundamental trade-off between energy efficiency and responsiveness. By combining event-driven operation with cooperative localization, the system activates anchors only when needed and allows *passive* tags to opportunistically utilize *active* tag localizations, reducing coordination overhead while maintaining centimeter-level accuracy and scalability.

The developed sensor nodes integrate WAKEMOD WuRs, QORVO DWM3000 UWB transceivers, and indoor solar energy harvesting, achieving ultra-low sleep power of $7.84 \mu\text{W}$ while remaining idle listening. Controlled experiments and real-world deployment on a quadruped robot confirm robust performance under varying conditions and sub-optimal anchor placement, with average localization errors of 21.89 cm for *active* tags, 25.70 cm for *passive* tags, and 43 cm in realistic dynamic scenarios.

Energy characterization and simulation studies demonstrate the system's sustainability and energy neutrality. *Active* tags consume 3.22 mJ per localization, *passive* tags 951 μJ , and anchors 353 μJ . The introduced energy-aware scheduling algorithm, based on AIMD principles, adapts localization rates to the availability of harvested solar energy, enabling up to 2031 localizations per tag per day under all conditions while maintaining 7% battery capacity on average for the nodes by the end of the simulated year, even when starting from an initial battery level of 0%.

ECO-WAKELOC enables maintenance-free, high-accuracy deployments in environments where wired infrastructure is impractical, such as already existing buildings, temporary installations, or large-scale IoT networks. Its cooperative and energy-adaptive design demonstrates that real-time indoor localization can achieve both low latency and energy-neutrality, paving the way for sustainable, cost-effective, and flexible deployments in a wide range of applications.

REFERENCES

[1] L.-W. Chen and C.-R. Chen, "Centimeter-level indoor positioning with facing direction detection for microlocation-aware services,"

IEEE Transactions on Systems, Man, and Cybernetics: Systems, vol. 54, no. 10, pp. 6458–6468, 2024. [Online]. Available: <http://dx.doi.org/10.1109/TSMC.2024.3432615>

[2] I. Silva, C. Pendao, and A. Moreira, “Real-world deployment of low-cost indoor positioning systems for industrial applications,” *IEEE Sensors Journal*, vol. 22, no. 6, pp. 5386–5397, 2022. [Online]. Available: <http://dx.doi.org/10.1109/JSEN.2021.3103662>

[3] I. E. Bouazzaoui, S. A. R. Florez, and A. E. Ouardi, “Enhancing rgbd slam performances considering sensor specifications for indoor localization,” *IEEE Sensors Journal*, vol. 22, no. 6, pp. 4970–4977, 2022. [Online]. Available: <http://dx.doi.org/10.1109/JSEN.2021.3073676>

[4] S. Hayward, K. van Lopik, C. Hinde, and A. West, “A survey of indoor location technologies, techniques and applications in industry,” *Internet of Things*, vol. 20, p. 100608, 2022. [Online]. Available: <http://dx.doi.org/10.1016/j.iot.2022.100608>

[5] A. K. Ramachandran Venkatapathy, A. Riesner, M. Roidl, J. Emmerich, and M. t. Hompel, “Phynode: An intelligent, cyber-physical system with energy neutral operation for phynetlab,” in *Smart SysTech 2015; European Conference on Smart Objects, Systems and Technologies*, 2015, pp. 1–8.

[6] P. Mayer, M. Magno, and L. Benini, “Self-sustaining ultrawideband positioning system for event-driven indoor localization,” *IEEE Internet of Things Journal*, vol. 11, no. 1, pp. 1272–1284, 2024. [Online]. Available: <http://dx.doi.org/10.1109/JIOT.2023.3289568>

[7] Y. Chen, Y. Wang, and Y. Zhao, “A room-level indoor localization using an energy-harvesting ble tag,” *Electronics*, vol. 13, no. 22, p. 4493, 2024. [Online]. Available: <http://dx.doi.org/10.3390/electronics13224493>

[8] M. Qi, B. Xue, and W. Wang, “Calibration and compensation of anchor positions for uwb indoor localization,” *IEEE Sensors Journal*, vol. 24, no. 1, pp. 689–699, 2024. [Online]. Available: <http://dx.doi.org/10.1109/JSEN.2023.3329535>

[9] R. Sayfoori, M.-H. Huang, A. Naderi, M. Bhatti, R. D. Frostig, and H. Cao, “High-precision uwb sensor-based real-time locating system for rodent behavioral studies,” *IEEE Sensors Journal*, vol. 25, no. 13, pp. 25 551–25 559, 2025. [Online]. Available: <http://dx.doi.org/10.1109/JSEN.2025.3572031>

[10] B. Yang, E. Yang, L. Yu, and A. Loeliger, “High-precision uwb-based localisation for uav in extremely confined environments,” *IEEE Sensors Journal*, vol. 22, no. 1, pp. 1020–1029, 2022. [Online]. Available: <http://dx.doi.org/10.1109/JSEN.2021.3130724>

[11] Y. Li, B. Yu, and L. Huang, “An indoor uwb localization method based on adaptive channel bias estimation,” *IEEE Sensors Journal*, vol. 25, no. 1, pp. 1339–1349, 2025. [Online]. Available: <http://dx.doi.org/10.1109/JSEN.2024.3493069>

[12] M. Bilge, “Evaluation of ultra wide band technology as an enhancement for ble based location estimation,” 2022. [Online]. Available: <https://arxiv.org/abs/2202.00558>

[13] G.-C. Pătru, L. Flueritoru, I. Vasilescu, D. Niculescu, and D. Rosner, “Flextdoa: Robust and scalable time-difference of arrival localization using ultra-wideband devices,” *IEEE Access*, vol. 11, pp. 28 610–28 627, 2023. [Online]. Available: <http://dx.doi.org/10.1109/ACCESS.2023.3259320>

[14] T. Laadung, S. Ulp, M. M. Alam, and Y. L. Moullec, “Novel active-passive two-way ranging protocols for uwb positioning systems,” *IEEE Sensors Journal*, vol. 22, no. 6, pp. 5223–5237, 2022. [Online]. Available: <http://dx.doi.org/10.1109/JSEN.2021.3125570>

[15] B. P. Sullivan, P. G. Yazdi, and S. Thiede, “Total cost of ownership of real-time locating system (rtls) technologies in factories,” *Procedia CIRP*, vol. 120, pp. 822–827, 2023. [Online]. Available: <http://dx.doi.org/10.1016/j.procir.2023.09.082>

[16] E. Zürich, “Polymaps indoor map application,” accessed: 20.09.2025. [Online]. Available: <https://ethz.ch/staffnet/en/organisation/departments/engineering-and-systems/polymaps.html>

[17] R. Ahmed, B. Buchli, S. Draskovic, L. Sigrist, P. Kumar, and L. Thiele, “Optimal power management with guaranteed minimum energy utilization for solar energy harvesting systems,” *ACM Transactions on Embedded Computing Systems*, vol. 18, no. 4, pp. 1–26, 2019. [Online]. Available: <http://dx.doi.org/10.1145/3317679>

[18] M. N. K. Boulos and G. Berry, “Real-time locating systems (rtls) in healthcare: a condensed primer,” *International Journal of Health Geographics*, vol. 11, no. 1, p. 25, 2012. [Online]. Available: <https://doi.org/10.1186/1476-072x-11-25>

[19] T. Istomin, E. Leon, D. Molteni, A. L. Murphy, G. P. Picco, and M. Griva, “Janus,” *Proceedings of the ACM on Interactive, Mobile, Wearable and Ubiquitous Technologies*, vol. 5, no. 4, pp. 1–33, 2021. [Online]. Available: <http://dx.doi.org/10.1145/3494978>

[20] T. Polonelli, S. Schlaper, and M. Magno, “Performance comparison between decawave dw1000 and dw3000 in low-power double side ranging applications,” in *2022 IEEE Sensors Applications Symposium (SAS)*, 8 2022. [Online]. Available: <http://dx.doi.org/10.1109/sas54819.2022.9881375>

[21] F. Villani, E. Masina, T. Burger, and M. Magno, “A 36nw ultra-wideband wake-up receiver with -86dbm sensitivity and addressing capabilities,” in *2024 IEEE International Symposium on Circuits and Systems (ISCAS)*, 5 2024, p. 5. [Online]. Available: <http://dx.doi.org/10.1109/ISCAS58744.2024.10558556>

[22] G. Kazdaridis, N. Sidiropoulos, I. Zografopoulos, and T. Korakis, “A novel architecture for semi-active wake-up radios attaining sensitivity beyond -70dbm: Demo abstract,” in *2021 20th International Conference on Information Processing in Sensor Networks*, 5 2021, pp. 398–399. [Online]. Available: <https://dx.doi.org/10.1145/3412382.3458782>

[23] G. Verma and V. Sharma, “A novel rf energy harvester for event-based environmental monitoring in wireless sensor networks,” *IEEE Internet of Things Journal*, vol. 9, no. 5, pp. 3189–3203, 2022. [Online]. Available: <http://dx.doi.org/10.1109/JIOT.2021.3097629>

[24] V. Luder, L. Schulthess, S. Cortesi, L. R. Davis, and M. Magno, “Anittrack: A power-efficient, time-slotted and robust uwb localization system for animal tracking in a controlled setting,” in *2025 10th International Workshop on Advances in Sensors and Interfaces (IWASI)*, 7 2025, pp. 1–6. [Online]. Available: <http://dx.doi.org/10.1109/IWASI66786.2025.11121986>

[25] M. Zhao, T. Chang, A. Arun, R. Ayyalasomayajula, C. Zhang, and D. Bharadia, “Uloc,” *Proceedings of the ACM on Interactive, Mobile, Wearable and Ubiquitous Technologies*, vol. 5, no. 3, pp. 1–31, 2021. [Online]. Available: <http://dx.doi.org/10.1145/3478124>

[26] S. Cortesi, C. Vogt, and M. Magno, “Wakeloc: An ultra-low power, accurate and scalable on-demand rtls using wake-up radios,” in *IEEE INFOCOM 2025 - IEEE Conference on Computer Communications Workshops (INFOCOM WKSHPS)*, 5 2025, pp. 1–6. [Online]. Available: <http://dx.doi.org/10.1109/INFOCOMWKSHPS65812.2025.11152965>

[27] D. Balsamo, A. S. Weddell, A. Das, A. R. Arreola, D. Brunelli, B. M. Al-Hashimi, G. V. Merrett, and L. Benini, “Hibernus++: a self-calibrating and adaptive system for transiently-powered embedded devices,” *IEEE Transactions on Computer-Aided Design of Integrated Circuits and Systems*, vol. 35, no. 12, pp. 1968–1980, 2016. [Online]. Available: <http://dx.doi.org/10.1109/TCAD.2016.2547919>

[28] D. Giouroukis, A. Dadiani, J. Traub, S. Zeuch, and V. Markl, “A survey of adaptive sampling and filtering algorithms for the internet of things,” in *Proceedings of the 14th ACM International Conference on Distributed and Event-based Systems*, 7 2020, pp. 27–38. [Online]. Available: <http://dx.doi.org/10.1145/3401025.3403777>

[29] M. Giordano, S. Cortesi, P.-V. Mekikis, M. Crabolu, G. Bellusci, and M. Magno, “Energy-aware adaptive sampling for self-sustainability in resource-constrained iot devices,” in *Proceedings of the 11th International Workshop on Energy Harvesting & Energy-Neutral Sensing Systems*, 11 2023. [Online]. Available: <http://dx.doi.org/10.1145/3628353.3628545>

[30] L. Schulthess, S. Cortesi, and M. Magno, “Wakemod: A 6.9 μ w wake-up radio module with -72.6 dbm sensitivity for on-demand iot,” in *2025 10th International Workshop on Advances in Sensors and Interfaces (IWASI)*, 7 2025, pp. 1–6. [Online]. Available: <http://dx.doi.org/10.1109/IWASI66786.2025.11122000>

[31] I. Dotlic, A. Connell, and M. McLaughlin, “Ranging methods utilizing carrier frequency offset estimation,” in *2018 15th Workshop on Positioning, Navigation and Communications (WPNC)*, 10 2018, p. 6. [Online]. Available: <http://dx.doi.org/10.1109/WPNC.2018.8555809>

[32] D. Coppers, A. Shahid, S. Lemey, B. V. Herbrugge, C. Marshall, and E. D. Poorter, “An overview of uwb standards and organizations (ieee 802.15.4, fira, apple): Interoperability aspects and future research directions,” *IEEE Access*, vol. 10, pp. 70 219–70 241, 2022. [Online]. Available: <http://dx.doi.org/10.1109/ACCESS.2022.3187410>

[33] M. Ridolfi, S. V. de Velde, H. Steendam, and E. D. Poorter, “Analysis of the scalability of uwb indoor localization solutions for high user densities,” *Sensors*, vol. 18, no. 6, p. 1875, 2018. [Online]. Available: <http://dx.doi.org/10.3390/s18061875>

[34] R. Ramesh, A. John-Sabu, H. S. S. Ramesh, V. N. B. M. Arunachalam, and B. Amruthur, “Robust and scalable techniques for twr and tdoa based localization using ultra wide band radios,” p. 6, 2020. [Online]. Available: <https://arxiv.org/abs/2008.04248>

[35] J. Yang, B. Dong, and J. Wang, “Vuloc,” *Proceedings of the ACM on Interactive, Mobile, Wearable and Ubiquitous Technologies*, vol. 6, no. 3, pp. 1–25, 2022. [Online]. Available: <http://dx.doi.org/10.1145/3550286>

[36] B. V. Herbruggen, D. V. Leemput, J. V. Landschoot, and E. D. Poorter, "Real-time anchor node selection for two-way-ranging (twr) ultra-wideband (uwb) indoor positioning systems," *IEEE Sensors Letters*, vol. 8, no. 3, pp. 1–4, 2024. [Online]. Available: <http://dx.doi.org/10.1109/LSENS.2024.3363231>

[37] P. Corbalán and G. P. Picco, "Ultra-wideband concurrent ranging," *ACM Transactions on Sensor Networks*, vol. 16, no. 4, pp. 1–41, 2020. [Online]. Available: <http://dx.doi.org/10.1145/3409477>

[38] B. Großwindhager, M. Stocker, M. Rath, C. A. Boano, and K. Römer, "Snaploc," in *Proceedings of the 18th International Conference on Information Processing in Sensor Networks*, 4 2019. [Online]. Available: <http://dx.doi.org/10.1145/3302506.3310389>

[39] L. Santoro, M. Nardello, D. Brunelli, and D. Fontanelli, "Scale up to infinity: the uwb indoor global positioning system," in *2021 IEEE International Symposium on Robotic and Sensors Environments (ROSE)*, 10 2021, p. 8. [Online]. Available: <http://dx.doi.org/10.1109/ROSE52750.2021.9611770>

[40] M. Spirito and A. Mattioli, "On the hyperbolic positioning of gsm mobile stations," in *1998 URSI International Symposium on Signals, Systems, and Electronics. Conference Proceedings (Cat. No.98EX167)*, 10 1998, p. 5. [Online]. Available: <http://dx.doi.org/10.1109/ISSSE.1998.738060>

[41] F. Gustafsson and F. Gunnarsson, "Positioning using time-difference of arrival measurements," in *2003 IEEE International Conference on Acoustics, Speech, and Signal Processing, 2003. Proceedings. (ICASSP '03)*, - 2003. [Online]. Available: <http://dx.doi.org/10.1109/ICASSP.2003.1201741>

[42] M. Kolakowski and V. Djaja-Josko, "Tdoa-twr based positioning algorithm for uwb localization system," in *2016 21st International Conference on Microwave, Radar and Wireless Communications (MIKON)*, 5 2016, pp. 1–4. [Online]. Available: <http://dx.doi.org/10.1109/MIKON.2016.7491981>

[43] C. Zhang, C. Tang, H. Wang, B. Lian, and L. Zhang, "Data set for uwb cooperative navigation and positioning of uav cluster," *Scientific Data*, vol. 12, no. 1, p. 486, 2025. [Online]. Available: <http://dx.doi.org/10.1038/s41597-025-04808-0>

[44] F. Sutton, B. Buchli, J. Beutel, and L. Thiele, "Zippy," in *Proceedings of the 13th ACM Conference on Embedded Networked Sensor Systems*, 11 2015. [Online]. Available: <http://dx.doi.org/10.1145/2809695.2809705>

[45] T. Polonelli, F. Villani, and M. Magno, "Ultra-low power wake-up receiver for location aware objects operating with uwb," in *2021 17th International Conference on Wireless and Mobile Computing, Networking and Communications (WiMob)*, 10 2021, p. 8. [Online]. Available: <http://dx.doi.org/10.1109/WiMob52687.2021.9606248>

[46] R. Piyare, A. L. Murphy, C. Kiraly, P. Tosato, and D. Brunelli, "Ultra low power wake-up radios: a hardware and networking survey," *IEEE Communications Surveys & Tutorials*, vol. 19, no. 4, pp. 2117–2157, 2017. [Online]. Available: <http://dx.doi.org/10.1109/COMST.2017.2728092>

[47] B. Chen, H. Ren, W. Gong, L. Lyu, and C.-J. Shi, "A 915mhz 97nw low-area wake-up receiver with an envelope-tracking mixer achieving -73.2dbm sensitivity," in *2025 IEEE International Symposium on Circuits and Systems (ISCAS)*, 5 2025, pp. 1–5. [Online]. Available: <http://dx.doi.org/10.1109/ISCAS56072.2025.11043883>

[48] M. Larsson, V. Larsson, K. Astrom, and M. Oskarsson, "Optimal trilateration is an eigenvalue problem," in *ICASSP 2019 - 2019 IEEE International Conference on Acoustics, Speech and Signal Processing (ICASSP)*, 5 2019, pp. 5586–5590. [Online]. Available: <http://dx.doi.org/10.1109/ICASSP.2019.8683355>

[49] M. Larsson, V. Larsson, K. Åström, and M. Oskarsson, "Single-source localization as an eigenvalue problem," *IEEE Transactions on Signal Processing*, vol. 73, pp. 574–583, 2025. [Online]. Available: <http://dx.doi.org/10.1109/TSP.2025.3532102>

[50] A. Beck, P. Stoica, and J. Li, "Exact and approximate solutions of source localization problems," *IEEE Transactions on Signal Processing*, vol. 56, no. 5, pp. 1770–1778, 2008. [Online]. Available: <http://dx.doi.org/10.1109/TSP.2007.909342>

[51] Y. Zhou, "A closed-form algorithm for the least-squares trilateration problem," *Robotica*, vol. 29, no. 3, pp. 375–389, 2010. [Online]. Available: <http://dx.doi.org/10.1017/S0263574710000196>

[52] D. R. Luke, S. Sabach, M. Teboulle, and K. Zatlawey, "A simple globally convergent algorithm for the nonsmooth nonconvex single source localization problem," *Journal of Global Optimization*, vol. 69, no. 4, pp. 889–909, 2017. [Online]. Available: <http://dx.doi.org/10.1007/s10898-017-0545-6>

[53] D. W. Marquardt, "An algorithm for least-squares estimation of nonlinear parameters," *Journal of the Society for Industrial and Applied Mathematics*, vol. 11, no. 2, pp. 431–441, 1963. [Online]. Available: <http://dx.doi.org/10.1137/0111030>

[54] J. J. Moré, *The Levenberg-Marquardt algorithm: Implementation and theory*, ser. Lecture Notes in Mathematics. Springer Berlin Heidelberg, 1978, ch. 10, pp. 105–116. [Online]. Available: <http://dx.doi.org/10.1007/BFb0067700>

[55] F. Jiang and A. Dhekne, "Demo: ufiμ: An open-source integrated uwb-wifi-imu platform for localization research and beyond," in *Proceedings of the 25th International Workshop on Mobile Computing Systems and Applications*, 2 2024, pp. 156–156. [Online]. Available: <http://dx.doi.org/10.1145/3638550.3643628>

[56] Y. Ding, D. Shen, K. Pham, and G. Chen, "Optimal placements for minimum gdop with consideration on the elevations of access nodes," *IEEE Transactions on Instrumentation and Measurement*, vol. 74, pp. 1–10, 2025. [Online]. Available: <http://dx.doi.org/10.1109/TIM.2024.3497055>

[57] D. Plozza, S. Marty, C. Scherrer, S. Schwartz, S. Zihlmann, and M. Magno, "Autonomous navigation in dynamic human environments with an embedded 2d lidar-based person tracker," in *2024 IEEE Sensors Applications Symposium (SAS)*, 7 2024, pp. 1–6. [Online]. Available: <http://dx.doi.org/10.1109/SAS60918.2024.10636369>

[58] D. Molteni, G. P. Picco, M. Tröbinger, and D. Vecchia, "Cloves" in *Proceedings of the 20th ACM Conference on Embedded Networked Sensor Systems*, 11 2022, pp. 808–809. [Online]. Available: <http://dx.doi.org/10.1145/3560905.3568072>

[59] L. Sigrist, A. Gomez, and L. Thiele, "Dataset: Tracing indoor solar harvesting," in *Proceedings of the 2nd Workshop on Data Acquisition To Analysis*, 11 2019, pp. 47–50. [Online]. Available: <http://dx.doi.org/10.1145/3359427.3361910>

[60] renata, "Rechargeable lithium-ion polymer batteries guidelines," accessed: 05.09.2025. [Online]. Available: <https://www.renata.com/en/downloadfile/renata-rechargeable-lipo-guidelines/?fileid=f871ff174d88fe997723e20ed>

[61] F. Malivert, O. Labbani-Igbida, and H. Boeglen, "Comparison and improvement of 3d-multilateration for solving simultaneous localization of drones and uwb anchors," *Applied Sciences*, vol. 13, no. 2, p. 1002, 2023. [Online]. Available: <http://dx.doi.org/10.3390/app13021002>

[62] D. Frisch and U. D. Hanebeck, "Why you shouldn't use tdoa for multilateration," in *Proceedings of the 2025 IEEE International Conference on Multisensor Fusion and Integration for Intelligent Systems (MFI 2025)*, College Station, Texas, September 2025, accessed: 08.12.2025. [Online]. Available: https://isas.iar.kit.edu/pdf/MFI25_Frisch.pdf

[63] R. Zandian and U. Witkowski, "Nlos detection and mitigation in differential localization topologies based on uwb devices," in *2018 International Conference on Indoor Positioning and Indoor Navigation (IPIN)*, 9 2018, pp. 1–8. [Online]. Available: <http://dx.doi.org/10.1109/IPIN.2018.8533781>



Silvano Cortesi (GS'22) received the B. Sc. and the M.Sc. degrees in electronics engineering and information technology from ETH Zürich, Zürich, Switzerland in 2020 and 2021, respectively. He is currently pursuing his Ph.D. degree with the Center for Project-Based Learning at ETH Zürich, Zürich, Switzerland. His research work focuses on indoor localization, ultra-low power and self-sustainable IoT, wireless sensor networks and energy harvesting.



Davide Plozza (GS'24) received the B.Sc. degree in electronics engineering and information technology in 2020 and the M.Sc. degree in robotics, systems and control in 2023, both from ETH Zürich, Switzerland. He is currently pursuing his Ph.D. degree with the Center for Project-Based Learning at ETH Zürich, Switzerland. His research focuses on robust navigation and locomotion for resource-constrained quadrupedal robots operating in harsh environments.



Lukas Schulthess (GS'22) received the Swiss Certificate of Competence (EFZ) as an electronic technician in 2014. He received the B.Sc. and the M.Sc. degrees in electronics engineering and information technology from ETH Zürich, Switzerland, in 2020 and 2021, respectively. He is currently pursuing a Ph.D. degree at ETH Zürich, Switzerland. His research interests include ultra-low power and miniaturized self-sustainable sensor nodes, wireless body area networks, and energy harvesting.



Christian Vogt (M'20) received the M.Sc. degree and the Ph.D. in electrical engineering and information technology from ETH Zürich, Zürich, Switzerland, in 2013 and 2017, respectively. He is currently a post-doctoral researcher and lecturer at ETH Zürich, Zürich, Switzerland. His research work focuses on signal processing for low power applications, including field programmable gate arrays (FPGAs), IoT, wearables and autonomous unmanned vehicles.



Michele Magno (SM'13) is currently a Senior Scientist at ETH Zürich, Switzerland, at the Department of Information Technology and Electrical Engineering. Since 2020, he is leading the D-ITET center for project-based learning at ETH. He received his master's and Ph.D. degrees in electronic engineering from the University of Bologna, Italy, in 2004 and 2010, respectively. He is working at ETH since 2013 and has become a visiting lecturer or professor at the University of Nice Sophia, Enssat Lannion, University of Bologna, and Mid Sweden University. His current research interests include smart sensing, low-power machine learning, wireless sensor networks, wearable devices, energy harvesting, and low-power management techniques. He has authored over 280 publications in international journals and conferences, earning best paper awards at IEEE events as well as recognition for industrial projects and patents.